ACS APPLIED MATERIALS & INTERFACES

Research Article

www.acsami.org

Magnetically Assisted Surface-Enhanced Raman Spectroscopy for the Detection of *Staphylococcus aureus* Based on Aptamer Recognition

Junfeng Wang,[†,§,⊥] Xuezhong Wu,[†,‡] Chongwen Wang,[§,#] Ningsheng Shao,[∥] Peitao Dong,[*,†,⊥] Rui Xiao,[*,§] and Shengqi Wang[*,§]

[†]College of Mechatronics and Automation and [‡]Laboratory of Science and Technology on Integrated Logistics Support, National University of Defense Technology, Changsha 410073, PR China

[§]Beijing Institute of Radiation Medicine, Beijing 100850, PR China

[∥]Beijing Institute of Basic Medical Sciences, Beijing 100850, PR China

[⊥]State Key Laboratory of Transducer Technology, Chinese Academy of Science, Shanghai 200050, PR China

[#]College of Life Sciences & Bio-Engineering, Beijing University of Technology, Beijing 100124, PR China

Supporting Information

ABSTRACT: A magnetically assisted surface-enhanced Raman scattering (SERS) biosensor for single-cell detection of *S. aureus* on the basis of aptamer recognition is reported for the first time. The biosensor consists of two basic elements including a SERS substrate (Ag-coated magnetic nanoparticles, AgMNPs) and a novel SERS tag (AuNR−DTNB@Ag−DTNB core−shell plasmonic NPs or DTNB-labeled inside-and-outside plasmonic NPs, DioPNPs). Uniform, monodisperse, and superparamagnetic AgMNPs with favorable SERS activity and magnetic responsiveness are synthesized by using polymer polyethylenimine. AgMNPs use magnetic enrichment instead of repeated centrifugation to prevent sample sedimentation. DioPNPs are designed and synthesized as a novel SERS tag. The Raman signal of DioPNPs is 10 times stronger than that of the commonly used SERS tag AuNR−DTNB because of the double-layer DTNB and the LSPR position adjustment to match the given laser excitation wavelength. Consequently, a strong SERS enhancement is achieved. Under the optimized aptamer density and linker length, capture by aptamer-modified AgMNPs can achieve favorable bacteria arrest (up to 75%). With the conventional Raman spectroscopy, the limit of detection (LOD) is 10 cells/mL for *S. aureus* detection, and a good linear relationship is also observed between the SERS intensity at Raman peak 1331 cm^{-1} and the logarithm of bacteria concentrations ranging from 10^1 to 10^5 cells/mL. With the help of the newly developed SERS mapping technique, single-cell detection of *S. aureus* is easily achieved.

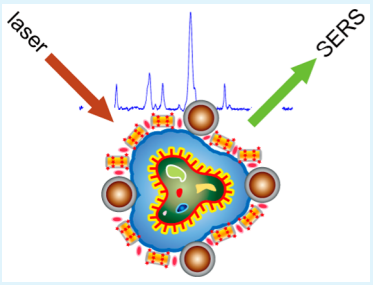

KEYWORDS: *surface-enhanced Raman spectroscopy, Staphylococcus aureus, single-cell detection, aptamer, Ag-coated magnetic nanoparticles*

1. INTRODUCTION

Staphylococcus aureus is an important human pathogen that can cause various diseases from less serious infections to life-threatening diseases such as abscesses, pneumonia, meningitis, endocarditis, and septicemia.[1,2] In addition, *S. aureus* can produce different enterotoxins that can cause food poisoning or can even be used as biochemical weapons. *S. aureus* is also one of the top five pathogens that cause food-borne illnesses worldwide. Therefore, the development of a rapid, sensitive, and specific detection method for *S. aureus* is highly important.

The time-consuming and laborious conventional detection method for *S. aureus* involves repeated enrichment, colony isolation, and various biochemical and serological identification tests. This process usually takes days to identify the pathogenic bacteria, and such a delay is unacceptable when facing emergencies, such as life-threatening diseases. Therefore, studies in the past decades focused on developing new detection methods for *S. aureus*, such as enzyme-linked immunosorbent assay, polymerase chain reaction amplification, and ligase chain reaction.[3−5] However, the complex procedures and high cost limit the widespread application of these technologies for clinical diagnosis.

Biosensor technology has undergone rapid development in recent years. Several biosensing technologies for the detection of *S. aureus* have been developed in the past few years; these techniques include electrochemical, fluorescence, colorimetric, light-scattering, two-photon Rayleigh scattering, and SERS methods.[2,6−12] Immunoassays based on antibody recognition have been well-established for several years.[9,13] However, the applications of antibodies are limited by their long selection

Received: July 16, 2015
Accepted: August 31, 2015
Published: August 31, 2015

DOI: 10.1021/acsami.5b06446
ACS Appl. Mater. Interfaces 2015, 7, 20919−20929

Scheme 1. Flowchart of *S. aureus* Detection Using SERS

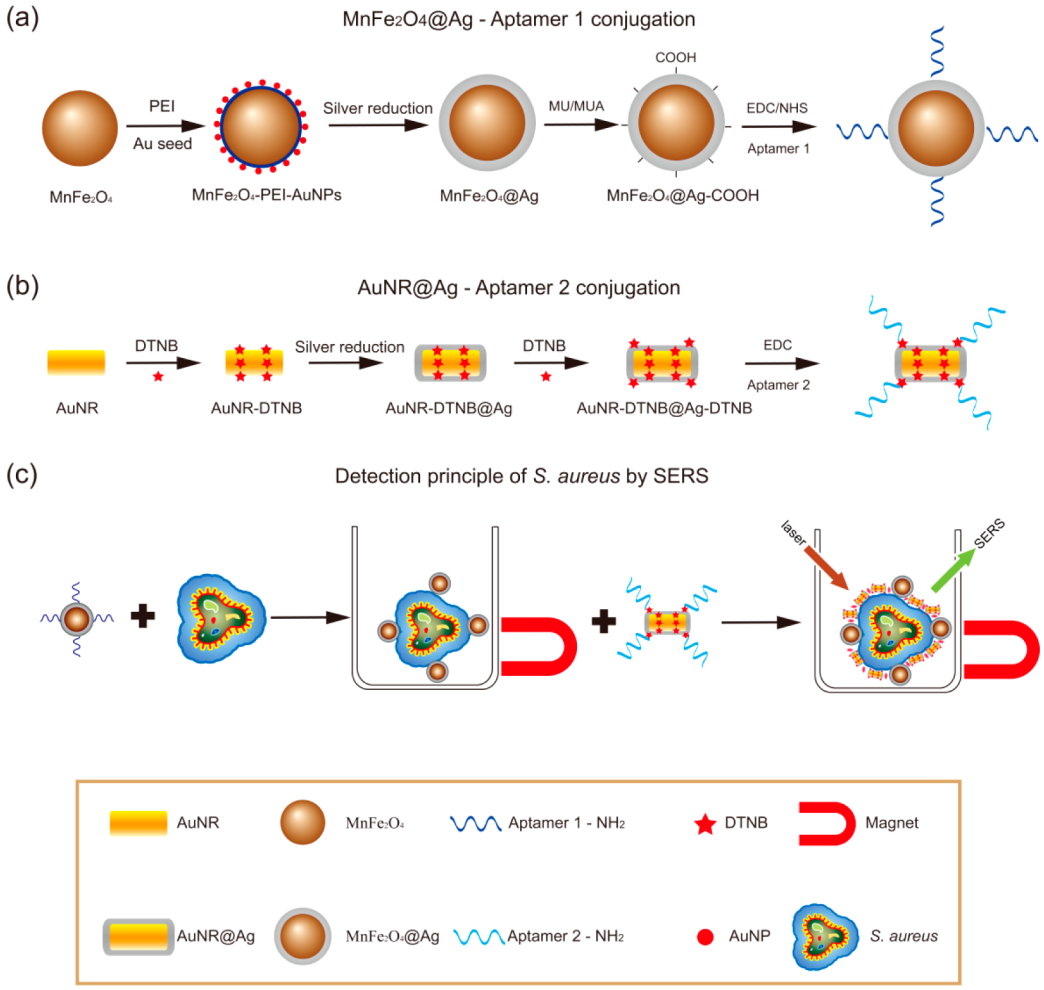

[a]Synthesis of monodispersed silver-coated magnetic nanoparticles and their conjugation with aptamer 1. [b]Synthesis of core−shell plasmonic nanoparticles (AuNR−DTNB@Ag−DTNB) and their conjugation with aptamer 2. [c]Schematic illustration of the operating principle for *S. aureus* detection.

process, high cost, low stability, and complicated modifications and conjugations. Aptamers are single-stranded DNA or RNA molecules that are commonly obtained through an in vitro selection process known as the systematic evolution of ligands by exponential enrichment (SELEX). Similar to antibodies, aptamers can bind to target bacteria with high affinity and specificity. However, aptamers possess several advantages over antibodies in both therapeutic and diagnostic applications. First, aptamers are obtained through in vitro selection. The universal SELEX process generally takes 2−3 months, with the quickest being 2 weeks. By contrast, the preparation of monoclonal antibodies requires at least 3−6 months and is costly. Second, aptamers are chemically synthesized and thus can be flexibly modified with multiple groups to make these molecules highly functional. Third, aptamers are much more chemically stable than antibodies. Antibodies are easily denatured because of their protein nature, whereas aptamers are chemically stable over a wide range of pH (2−12) and have a certain degree of thermal annealing features. Aptamers have been widely used to detect bacteria or even cancer cells.[2,6−8,14,15] However, to the best of our knowledge, aptamers have not been used in SERS assays for *S. aureus*.

SERS spectroscopy is an important analytical technique for biological sensing and trace analysis because of the enormous Raman enhancement.[16−24] Given its high sensitivity and fingerprinting capability, SERS has been applied in various fields.[25−27] The detection and identification of pathogenic microorganisms by SERS have recently attracted interest because of the potential application of this technology in single-cell detection.[2] The SERS enhancement substrate and the SERS tag are important basic elements for the extrinsic detection mode of SERS; these elements can produce strong, characteristic Raman signals to sense indirectly the target molecules.[28]

Ag-coated magnetic nanoparticles (AgMNPs) have attracted considerable attention in SERS detection application because of the high SERS activity of Ag shell, good magnetic responsiveness of magnetic core, and relatively facile fabrication process.[29,30] At present, AgMNPs are commonly synthesized with the help of an interlayer of silica shells to prevent the aggregation of the magnetic NPs and provide numerous surface Si−OH groups for further modification. For example, Hu et al. used the Ag-mirror reaction to deposite in situ AgNPs on the surfaces of Fe_3O_4@SiO_2 composite microspheres.[31] Han et al. used the "seed-mediated growth" method to form an Ag shell on the surfaces of Fe_3O_4@SiO_2 microspheres.[32] However, the

DOI: 10.1021/acsami.5b06446
ACS Appl. Mater. Interfaces 2015, 7, 20919−20929

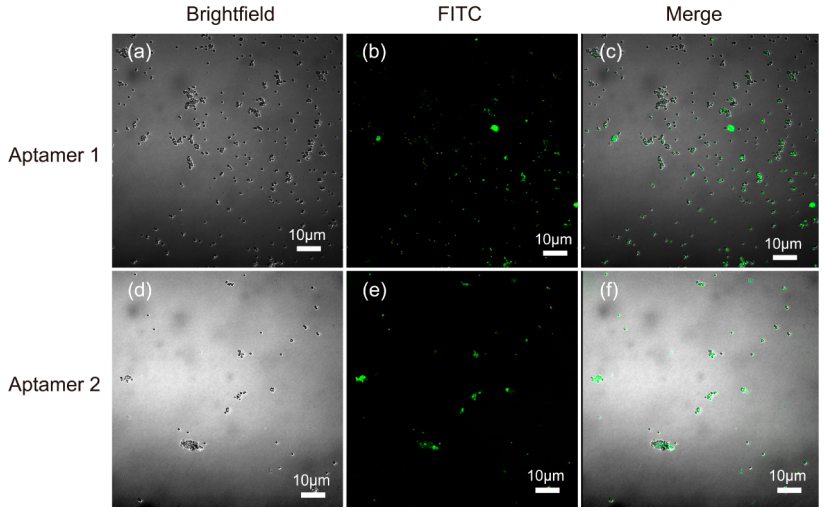

Figure 1. Confocal fluorescence micrographs of *S. aureus* (04018) binding to different aptamers. (a and d) Brightfield, (b and e) fluorescence, and (c and f) merged images of *S. aureus* binding with the FITC-labeled (a–c) aptamer 1 and (d–f) aptamer 2, respectively.

presence of silica shells considerably affects the magnetic responsiveness and increases structural size. Moreover, these methods form a noncontinuous Ag shell, which affects SERS activity. Therefore, the synthesis of magnetic NPs with a continuous Ag shell that exhibits good dispersity and strong magnetic responsiveness remains a challenge.

SERS tags are widely used for the extrinsic mode of SERS detection.[33,34] As reviewed by Wang et al., the SERS tag was developed from the simple metal-nanosphere–Raman-reporter structure to the plasmonic nanoparticle (PNP)–Raman-reporter structure.[19] Au or Ag nanosphere–Raman-reporter conjugates are easy to synthesize. However, the maximum localized surface plasmon resonance (LSPR) position of both types is limited to approximately 400–600 nm, and the signal is easily disturbed by surrounding interference. PNPs have an LSPR wavelength that can be freely adjusted as needed. Commonly used PNPs are bimetallic Au@Ag core–shell NPs, including Au@Ag nanospheres, Au@Ag nanorods, Au@Ag shells, and Au@Ag nanocages. These structures take advantage of the high SERS activity of Ag and the homogeneous superiority of Au. Adjusting the thickness of Ag shell can continuously tune the LSPR wavelength of the bimetallic NPs in a wide range from that of Au cores to Ag shells, which allows a match with the given laser excitation wavelength to achieve a strong SERS enhancement. Subsequently, PNPs were modified with Raman reporters and target recognition molecules to form a plasmonic SERS tag. However, a universal plasmonic SERS tag that exhibits a high SERS activity and conveniently conjugates with target recognition molecules (antibody or aptamer) remains to be synthesized.

In the current study, a magnetically assisted SERS biosensor for single-cell detection of *S. aureus* that is based on aptamer recognition was proposed and constructed for the first time to the best of our knowledge. Superparamagnetic magnetic NPs ($MnFe_2O_4$, ~170 nm) with good dispersity and strong magnetic responsiveness were synthesized through a binary solvent solvothermal reaction. Subsequently, AgMNPs approximately 200 nm in diameter were successfully synthesized through the seed-mediated growth method to form a continuous Ag shell outside the magnetic cores. In addition, we designed a novel SERS tag (DTNB-labeled inside-and-outside plasmonic NPs or DioPNPs) that exhibits a high SERS activity and conveniently conjugates with target recognition molecules (antibody or aptamer). Finally, the detection of *S. aureus* was achieved by SERS method.

2. RESULTS AND DISCUSSION

2.1. Operating Principle of SERS Biosensor for *S. aureus* Detection on the Basis of Aptamer Recognition. Antibodies and aptamers are widely used recognition elements for the specific capture of whole bacteria. Our designed detection method for bacteria is based on aptamer recognition considering the above-mentioned advantages of aptamers.

Scheme 1c represents the operating principle of the SERS biosensor for bacteria detection that is based on aptamer recognition. Similar to the immunoassay platform, which employs the sandwich-type configuration of antibody/antigen/antibody, our designed SERS biosensor is also based on a sandwich structure formed by aptamer/target/aptamer interactions.[18] The SERS biosensor included two processes carried out in 1.5 mL microtubes. First, mixtures of aptamer-1-conjugated AgMNPs and *S. aureus* were incubated for binding; during incubation, *S. aureus* bound to the aptamer-1-modified AgMNPs. The resultant solution was subsequently subjected to magnetic confinement and turned from cloudy to clear within approximately 2 min, indicating the very strong binding interaction between aptamer-1-modified AgMNPs and *S. aureus*. Second, the resulting bacteria–AgMNPs complexes were magnetically separated and rinsed with PBST to remove the excessive free bacteria. Afterward, aptamer-2-conjugated DioPNPs were added and incubated for binding. *S. aureus* has different binding sites for aptamers 1 and 2; thus, the bacteria can bind to the capture aptamer and detection aptamer simultaneously, leading to the formation of the DioPNPs/*S. aureus*/AgMNPs sandwich architecture. After washing with PBST under magnetic confinement to remove the free DioPNPs, the resultant DioPNPs/*S. aureus*/AgMNPs complexes were resuspended in ethanol and dropped on a silicon substrate. After drying in air, SERS spectroscopy and imaging were conducted.

2.2. Characterization of the Binding Ability of Aptamers to Bacteria. The binding ability of aptamers to *S. aureus* is the key feature of our designed biosensor because it determines the formation of sandwich structure. Thus, we

DOI: 10.1021/acsami.5b06446
ACS Appl. Mater. Interfaces 2015, 7, 20919–20929

studied the binding ability of free aptamers to *S. aureus*. Two FITC-labeled aptamers were respectively incubated with *S. aureus* (04018) suspension. During incubation, the aptamers opened their secondary structure (Figure S1) and bound to *S. aureus* in the presence of Mg^{2+} (5 mM). After the unbound free FITC-labeled aptamers were removed, the bacteria−aptamers sediment was resuspended in ethanol, dropped on a glass slide, and then visualized under a confocal laser-scanning microscope (Figure 1). As shown in Figure 1, aptamers 1 and 2 exhibit favorable binding ability to *S. aureus*.

2.3. Synthesis of Ag-Coated Magnetic NPs and Their Conjugation with Aptamers. Immunomagnetic beads have been used to capture and detect viruses, bacteria, and tumor cells.[9,35,36] Similar to these immunomagnetic beads, our designed aptamer-modified AgMNPs were used for the capture and SERS detection of *S. aureus*. As shown in Figure S2, the mean diameter of *S. aureus* cultured overnight is approximately 650 nm. Thus, AgMNPs approximately 200 nm in diameter were designed and synthesized to detect *S. aureus* in consideration of the steric hindrance during magnetic bead−bacteria binding and the speed issue of magnetic enrichment.

Superparamagnetic manganese ferrite NPs ($MnFe_2O_4$, ~ 170 nm) were synthesized through a binary solvent solvothermal reaction with polyvinylpyrrolidone (PVP) as surfactant as described by Leung.[37] $FeCl_3$ and $MnCl_2$ were used as precursors, and a mixture of EG/DEG acted as both the solvent and reductant. NaOAc was selected for electrostatic stabilization to prevent particle agglomeration. NaOAc can also increase the alkalinity of reaction system after hydrolysis, which promotes the hydrolysis of $FeCl_3$ and $MnCl_2$ to form $Fe(OH)_3$ and $Mn(OH)_2$, respectively. Finally, $MnFe_2O_4$ NPs were formed after dehydration. The synthesized $MnFe_2O_4$ NPs were highly dispersible in solution because of the absence of dominant crystal planes that cause adhesion between the surfaces of the NPs.

The seed-mediated growth method was used to form a continuous Ag shell outside the $MnFe_2O_4$ NPs. The in-process product $MnFe_2O_4$@PEI−AuNPs were obtained via the electrostatic interaction between the primary amine groups of PEI wrapped outside the $MnFe_2O_4$ NPs and the 4 nm negatively charged Au seeds. Under the stabilization of PVP, a formaldehyde and ammonia solution was used to reduce $AgNO_3$ within a few seconds to form a continuous Ag shell outside the magnetic NPs with the Au seeds as nuclei.

The size and shape of the as-obtained samples were characterized via transmission electron microscopy (TEM) and scanning electron microscopy (SEM). Figure 2a,b shows the TEM images of $MnFe_2O_4$ NPs, whereas Figure 2c shows the SEM image of $MnFe_2O_4$ NPs. The prepared monodisperse spherical $MnFe_2O_4$ NPs had a diameter of approximately 170 nm. The prepared $MnFe_2O_4$ NPs were composed of many smaller NPs, and their surfaces were rough as shown in Figure 2c. Figure 2d−f shows the electron micrographs of the in-process product $MnFe_2O_4$@PEI−AuNPs. It can be clearly seen from the HRTEM image (inset image of Figure 2e) that several AuNPs were clearly absorbed outside the $MnFe_2O_4$ NPs. The absorption of AuNPs was also confirmed through energy dispersive spectroscopy (EDS) of $MnFe_2O_4$@PEI−AuNPs (Figure S3). Mn, Fe, O, and Au were all present in the EDS spectra of these NPs; C and Cu were derived from the carbon-supported copper TEM grid. Figure 2g−i shows the electron micrographs of the prepared Ag-coated magnetic NPs ($MnFe_2O_4$@Ag), and the diameter of the prepared

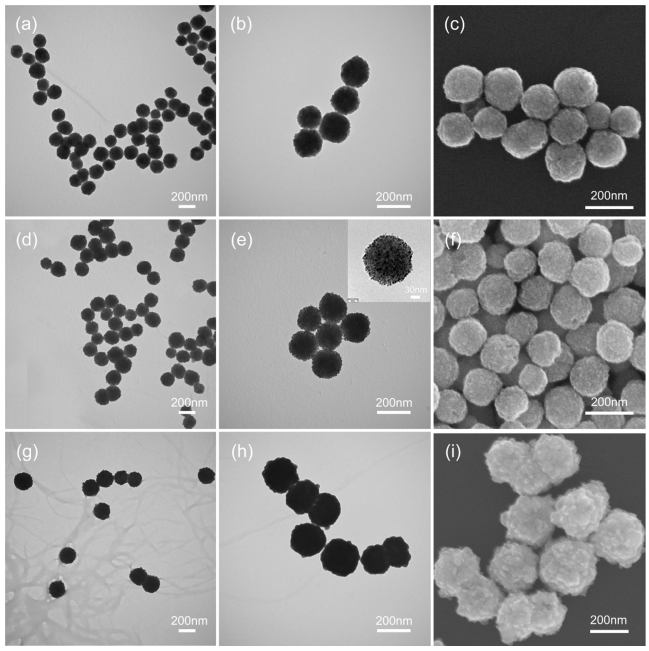

Figure 2. TEM and SEM images of the synthesized magnetic nanoparticles. (a−c) $MnFe_2O_4$, (d−f) $MnFe_2O_4$@PEI−AuNPs, and (g−i) $MnFe_2O_4$@Ag. (a, d, and g) 50× TEM, (b, e, and h) 100× TEM, and (c, f, and i) SEM images.

$MnFe_2O_4$@Ag was approximately 200 nm. The Ag shell formation progressed from discontinuous to continuous outside the $MnFe_2O_4$ NPs and was investigated by controlling the amount of $AgNO_3$ (Figure S4). As described in the Experimental Methods section, the amount of PVP was maintained at 300 mg, whereas that of $AgNO_3$ varied from 1 to 4 mg. Figure S4 shows the TEM images of $MnFe_2O_4$@Ag at different concentrations of $AgNO_3$. When a small amount of $AgNO_3$ (e.g., 1 or 1.5 mg) was added, Ag^+ was reduced on the surface of the absorbed AuNPs but not in amounts large enough to form a continuous shell (Figure S4a,b). When the amount of $AgNO_3$ was increased to 2.5 mg, the resulting Ag shell became slightly rough but basically continuous (Figure S4c). Furthermore, the Ag shell became absolutely continuous when 4 mg of $AgNO_3$ was added.

The as-obtained samples were also examined by X-ray diffraction (XRD) (Figure 3a). The XRD peaks of the synthesized $MnFe_2O_4$ can be indexed to the Powder Diffraction File (PDF) database (PDF 74-2403, International Centre for Diffraction Data (ICDD), 2004). The peaks of $MnFe_2O_4$ (curve a, Figure 3a) can be clearly observed at 2θ values of 29.6, 35.1, 42.5, 52.6, 56.1, and 61.6, which corresponded to the reflections of the (220), (311), (400), (422), (511), and (440) crystalline planes of the synthesized $MnFe_2O_4$. After the absorption of AuNPs on the $MnFe_2O_4$ NPs, a new XRD peak (curve b, Figure 3a) was observed at a 2θ value of 38.2, which corresponded to the (111) crystalline plane of Au (PDF 04-0784, ICDD, 2004). After the continuous Ag shell was formed outside the $MnFe_2O_4$ NPs, five new peaks of Ag (curve c, Figure 3a) were clearly observed at 2θ values of 38.1, 44.3, 64.4, 77.5, and 81.5, which corresponded to the reflections of the (111), (200), (220), (311), and (222) crystalline planes of the synthesized Ag shell (PDF 04-0783, ICDD, 2004).

The magnetic properties of the synthesized $MnFe_2O_4$, $MnFe_2O_4$@PEI−AuNPs, and $MnFe_2O_4$@Ag NPs were inves-

DOI: 10.1021/acsami.5b06446
ACS Appl. Mater. Interfaces 2015, 7, 20919−20929

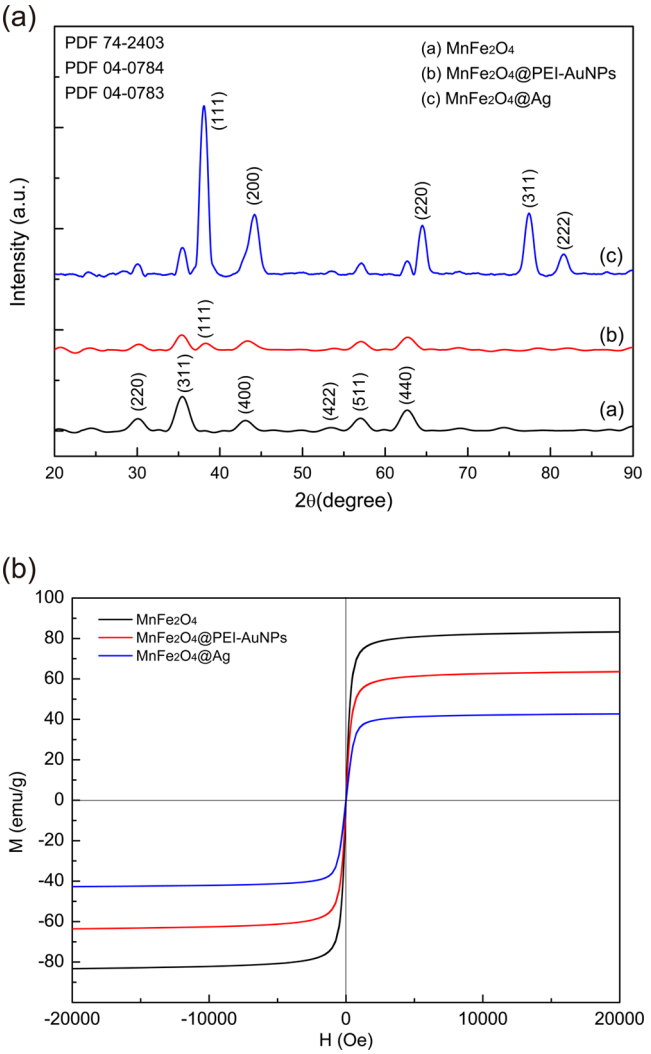

Figure 3. (a) XRD patterns and (b) magnetic hysteresis curves of $MnFe_2O_4$, $MnFe_2O_4$@PEI−AuNPs, and $MnFe_2O_4$@Ag.

tigated with a SQUID magnetometer at 300 K (Figure3b). Hysteresis loops were absent for all the synthesized NPs at 300 K, which indicated that all of the NPs exhibited superparamagnetic properties.[30] The superparamagnetic property can prevent aggregation and enable the magnetic nanoparticles to rapidly redisperse when the magnetic field is removed; thus, this property is critical for the applications of these NPs in the biomedical field. The magnetic saturation (MS) values are 83.4, 63.5, and 42.7 emu/g for $MnFe_2O_4$, $MnFe_2O_4$@PEI−AuNPs, and $MnFe_2O_4$@Ag NPs, respectively. The decrease in the overall MS values indicated that the $MnFe_2O_4$ surface was covered with nonmagnetic materials, such as PEI, AuNPs, and Ag, as confirmed by the TEM and SEM images. Such excellent magnetic properties implied that the synthesized $MnFe_2O_4$@Ag NPs had strong magnetic responsivity and can be easily separated from the solution with the help of an external magnetic force within approximately 2 min.

Figure S5 showed the UV−vis spectra of the synthesized $MnFe_2O_4$, $MnFe_2O_4$@PEI−AuNPs, and $MnFe_2O_4$@Ag NPs. Upon the formation of the Ag shell, the absorbance peak red-shifted to approximately 420 nm because of the Mie plasmon resonance excitation from the AgNPs.

AgMNPs ($MnFe_2O_4$@Ag) were conjugated with amino aptamer 1 via the EDC/NHS method.[38] In brief, the AgMNPs were carboxylated through the treatment of MUA/MU at a 1:1 ratio. After washing, EDC and NHS were added to form active ester that can rapidly couple with amines on target aptamers. The binding of aptamers to AgMNPs was investigated through in situ PCR amplification, as shown in Figure S6. The bright bands corresponding to 88 bp indicate that the aptamers have been well-modified on the AgMNP surfaces.

2.4. Synthesis of Au Nanorod−DTNB@Ag−DTNB Core−Shell Plasmonic NPs and their Conjugation with Aptamers. The SERS tag was typically composed of a metal nanosubstrate, an organic Raman reporter molecule, a protection shell, and targeting molecules. It is commonly used to label and detect a target. In the present study, we designed a novel SERS tag (DioPNPs), shown in Scheme 1b. DioPNPs possessed various advantages over the commonly used SERS tag based on AuNPs and AgNPs. First, the LSPR wavelength of DioPNPs can be freely adjusted from the visible to near-infrared (NIR; Figure S7) as required. For the detection of biological samples, a NIR wavelength (for example 780 nm) was preferred by considering the issues of reducing background autofluorescence and sample damage. Second, the SERS signal of DioPNPs is strong and stable. DioPNPs consist of two layers of DTNB molecules; the inner layer is encapsulated by a Ag shell that prevents it from being washed to ensure the signal stability. Finally, DioPNPs can conveniently conjugate with antibodies or amino aptamers. The outer layer DTNB on DioPNPs is bifunctional, acting as a Raman reporter and a linker for antibodies or other targets with amino groups.

AuNRs typically exhibiting an LSPR of 840 nm, which corresponds to an aspect ratio of approximately 4, were obtained using the seed-mediated method developed by Nikoobakht with some modifications.[39] The synthesized AuNRs were characterized via TEM with dimensions of approximately 72 nm × 18 nm (Figure 4a). AuNRs with a few irregular large particles were successfully synthesized by adding a proper amount of HCl. These AuNRs were modified with 10 μM DTNB under sonication for 1 h. After removing the excess DTNB through centrifugation, the DTNB-modified AuNRs were encapsulated with a Ag shell by using a previously reported method with some modifications.[40] The LSPR wavelength blue-shifted after Ag shell encapsulation. AuNR−DTNB@Ag with an LSPR wavelength of 780 nm, which was consistent with the laser wavelength used for detection, was successfully synthesized (Figure 4b). The inset of Figure 4b shows that the Ag shell thickness was approximately 1.5 nm, consistent with the simulation results (Figure S8). In addition, the formation of Ag shell outside DTNB-modified AuNRs was also confirmed by the EDS spectrum of AuNR−DTNB@Ag (Figure S9): Au and Ag were present, whereas Cu was derived from the carbon-supported copper TEM grid. The resulting AuNR−DTNB@Ag NPs were modified with 10 μM DTNB again under sonication for 1 h to form the AuNR−DTNB@Ag−DTNB core−shell plasmonic NPs, or the so-called DioPNPs.

Figure 4c shows the UV−vis spectra of the synthesized AuNR, AuNR−DTNB, AuNR−DTNB@Ag, and AuNR−DTNB@Ag−DTNB NPs. The figure shows that DTNB exerted no influence on the LSPR wavelength of AuNR or AuNR−DTNB@Ag NPs. Upon the formation of a Ag shell, the LSPR blue-shifted from 840 nm to approximately 780 nm. Figure 4d shows the Raman spectra of the synthesized AuNR−

DOI: 10.1021/acsami.5b06446
ACS Appl. Mater. Interfaces 2015, 7, 20919−20929

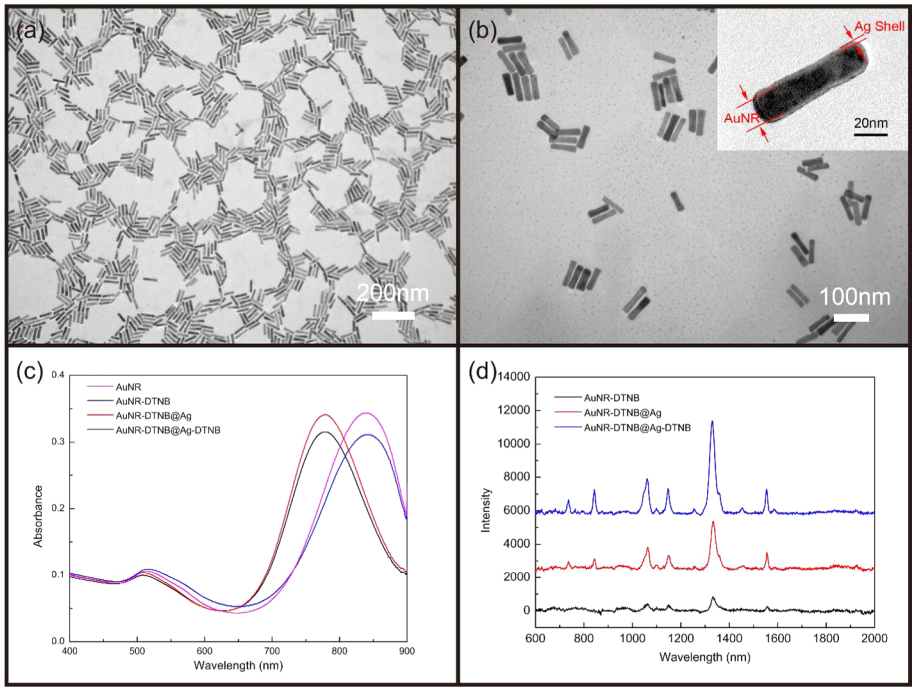

Figure 4. TEM images of (a) the synthesized AuNRs and (b) the AuNR−DTNB@Ag core−shell plasmonic nanoparticles. The inset in b is an HRTEM image of a single AuNR−DTNB@Ag nanoparticle. (c) UV−visible spectra of the synthesized nanoparticles. (d) Raman intensity of AuNR−DTNB, AuNR−DTNB@Ag, and AuNR−DTNB@Ag−DTNB under the same conditions.

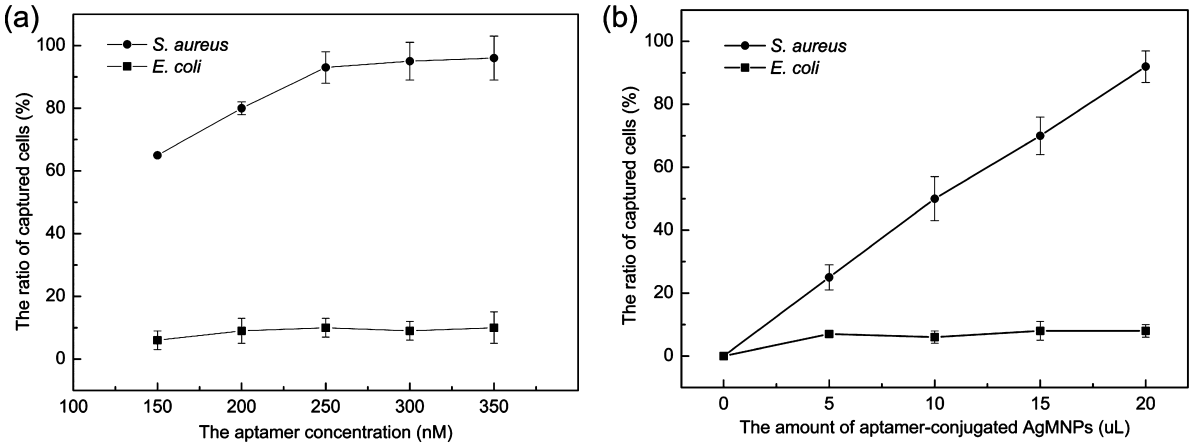

Figure 5. Curves of the captured cells ratio versus (a) aptamer concentration and (b) amount of aptamer-conjugated AgMNPs with 45 min interaction time for *S. aureus* and *E. coli* cells.

DTNB, AuNR−DTNB@Ag, and AuNR−DTNB@Ag−DTNB NPs. The signal of our newly−designed SERS tag (DioPNPs) was clearly approximately 10 times stronger than that of AuNR−DTNB NPs.

DioPNPs were conjugated with amino aptamer 2 through standard EDC coupling[11] between the DTNB−COOH group and amino group of the aptamer. Unlike the carboxyl activation method via EDC/NHS for carboxylated AgMNPs, the standard EDC method was used to activate the carboxyl groups of the outer layer DTNB on DioPNPs considering the NPs were easy to agglomerate together because of a high concentration of salt. After activation, DioPNPs can rapidly couple with amines on target aptamers.

2.5. Characterization of the Capture Ability of Aptamer-Conjugated AgMNPs to Bacteria. As illustrated in Figure 1, both aptamers 1 and 2 displayed a favorable binding ability to *S. aureus* in their free state. Once the aptamers were bound to AgMNPs, two key factors determined the ability of aptamers to capture bacteria. These factors are the density and linker length of the aptamers modified on AgMNPs. If the aptamers are too dense, then interference occurs between adjacent aptamers. This occurrence prevents the secondary structure of aptamer from being open. By contrast, if the aptamers are too sparse, then bacteria cannot be firmly captured. Equally important is the linker length, which plays an important role in the effective capture of *S. aureus*. If the linker is too short, then bacteria cannot be captured because of the steric hindrance. If the linker is too long, then the stiffness is not sufficient to ensure effective capture.

Two plans were considered for the conjunction of aptamers to AgMNPs. In the first plan, streptavidin (SA)-functionalized AgMNPs were used to conjugate the biotin-labeled aptamer

DOI: 10.1021/acsami.5b06446
ACS Appl. Mater. Interfaces 2015, 7, 20919−20929

through the SA−biotin interaction with good affinity and specificity. However, this plan has some disadvantages. First, the density of aptamer can only be adjusted by changing the concentration of aptamer used. Second, the linker can only be added by extending the length of the aptamer, thereby increasing the cost and difficulty of the artificial synthesis of aptamers. In addition, the orientation of aptamers cannot be guaranteed because each SA molecule contains four biotin binding sites, which may explain why the secondary structure of aptamers cannot be opened. This plan was finally discarded because of the above-mentioned disadvantages and because the practical capture effect was very poor (data not shown).

The second plan for the conjunction of aptamers to AgMNPs is shown in Scheme 1a. This plan was finally used because of its various advantages over the previously used one. MU/MUA (1:1) was used to form carboxylated AgMNPs. This surface modification carboxylated one-half of the AgMNP surface area and subsequently adjusted the aptamer density. Meanwhile, the carbon chains of MUA functioned as linkers, which protected the amino aptamer from being added with some bases (such as 10 T) that were used as linker. In addition, the EDC/NHS method, which was used to conjugate the aptamers to AgMNPs, was very reliable and convenient.

To obtain the optimized concentration of the aptamers, different concentrations (100, 150, 200, 250, 300, and 350 nM) were used to conjugate with AgMNPs and to detect the same sample (10^6 cfu/mL *S. aureus*) with *E. coli* as contrast. Subsequently, the resulting bacteria−AgMNPs complexes were magnetically separated, and the absorbance of the supernatant at 600 nm, which corresponded to the concentration of bacteria, was measured. The ratio of captured cells was obtained as shown in Figure 5a. With 150 nM aptamer concentration, 65% *S. aureus* cells were captured, and more than 93% *S. aureus* cells were captured over 250 nM. In contrast, *E. coli* cells showed little adhesive capacity to aptamer-conjugated AgMNPs, and less than 10% of cells were captured for all the concentrations. Therefore, 250 nM was selected as the optimized concentration of aptamer.

To obtain the optimized dosage of aptamer-1-conjugated AgMNPs (5 mg/mL), different amounts of aptamer-1-conjugated AgMNPs (5, 10, 15, and 20 μL) were used to capture the same sample (10^6 cfu/mL *S. aureus*). As shown in Figure 5b, with the increase of dosage, the amount of captured *S. aureus* cells increased, and the relationship between dosage and captured cells was almost linear. However, no matter how many the aptamer-conjugated AgMNPs were used, few *E. coli* cells could be captured, and the captured amount did not exceed 10%. The vast difference between these two types of cells should be ascribed to specificity of the aptamer recognition. In *S. aureus* cells, with the assistance of this recognition, the more aptamer-conjugated AgMNPs used, the more cells were separated by an external magnetic field. Meanwhile, the resulting *S. aureus*−AgMNPs complexes were investigated via TEM (Figure 6). The figure shows that the number of AgMNPs conjugated outside *S. aureus* increases as the amount of aptamer-1-conjugated AgMNPs increases. The more AgMNPs conjugated outside *S. aureus*, the quicker magnetic enrichment was achieved. However, enough space must be spared for the attachment of aptamer-2-conjugated DioPNPs. Despite the cell capture rate being only approximately 75%, 15 μL (Figure 6c) was selected as the optimized amount of aptamer-1-conjugated AgMNPs for the detection of *S. aureus*.

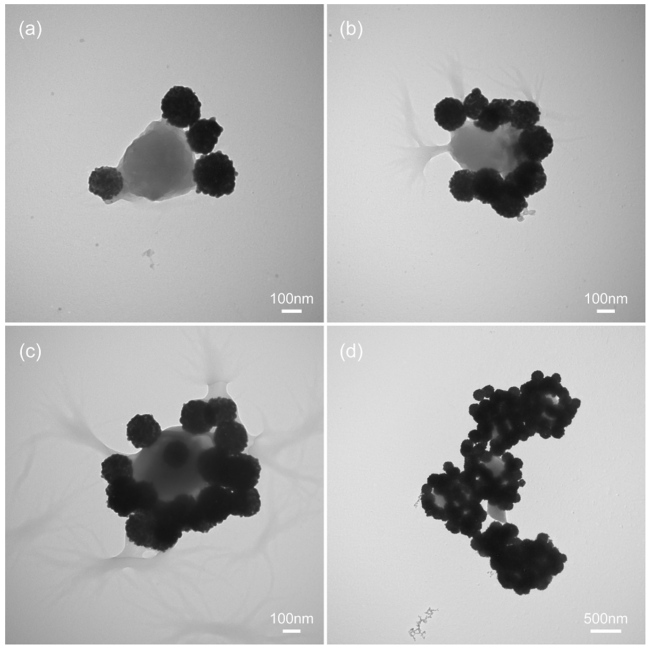

Figure 6. TEM images of the capture results by (a) 5 μL, (b) 10 μL, (c) 15 μL, and (d) 20 μL of aptamer-1-conjugated AgMNPs to capture the same *S. aureus* sample (10^6 cfu/mL).

2.6. Detection of *S. aureus* by SERS. After *S. aureus* was captured by aptamer-1-conjugated AgMNPs, aptamer-2-conjugated DioPNPs were added and incubated to form the DioPNPs/*S. aureus*/AgMNPs sandwich architecture (Figure S10). It can be obviously seen from the figure that several DioPNPs were conjugated outside *S. aureus*. Subsequently, Raman spectroscopy and imaging were conducted using a Raman imaging microscope equipped with a 780 nm laser, which was consistent with the LSPR wavelength of the DioPNPs.

The SERS spectra for *S. aureus* assays conducted by using the novel DioPNPs are shown in Figure 7a, and they display the typical SERS response of the sensing platform after the addition of various concentrations of *S. aureus*. The spectra contain features attributable to the Raman reporter molecule (DTNB) introduced by the DioPNPs and are dominated by the main Raman peak at 1331 cm^{-1} that belongs to the symmetric nitro stretch mode. The detection is based on a characteristic feature of the SERS tag and then quantified by its intensity. The calibration curve between the SERS intensity at Raman peak 1331 cm^{-1} and the logarithm of *S. aureus* bacteria concentrations (10^1−10^5 cells/mL) was plotted. The SERS signal becomes weaker as the concentration decreases and can be distinguished when bacreria concentration down to 10 cells/mL, so the LOD of the proposed biosensor for *S. aureus* is 10 cells/mL. Besides, a good linear relationship is observed from 10^1 to 10^5 cells/mL *S. aureus* concentration, and the correlation coefficient is calculated to be 0.9558.

The LOD of the proposed biosenser for *S. aureus* using conventional Raman spectroscopy is 10 cells/mL; however, with the help of newly developed SERS mapping technique, single-cell detection can be easily achieved. Figure 8a shows the SEM image of a single *S. aureus* cell labeled with either AgMNPs and DioPNPs or the DioPNPs/*S. aureus*/AgMNPs sandwich architecture. Figure 8b shows the corresponding optical image of the DioPNPs/*S. aureus*/AgMNPs sandwich

DOI: 10.1021/acsami.5b06446
ACS Appl. Mater. Interfaces 2015, 7, 20919−20929

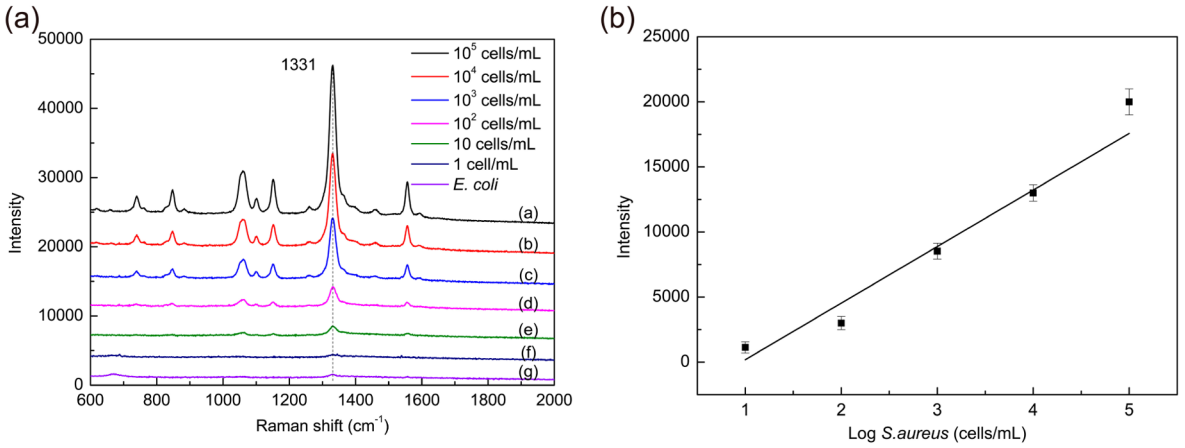

Figure 7. (a) SERS spectra taken from the DioPNPs/bacteria/AgMNPs sensing platform with various concentrations of *S. aureus* (10^5, 10^4, 10^3, 10^2, 10^1, and 10^0 cells/mL) and *E. coli* (10^5 cells/mL). (b) Calibration curve for *S. aureus* at a concentration range of 10^1−10^5 cells/mL obtained by using SERS intensity at 1331 cm^{-1}.

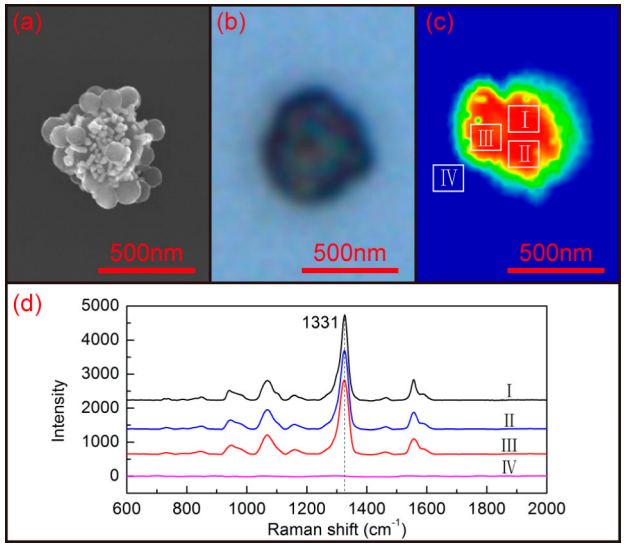

Figure 8. Single-cell detection of *S. aureus* by SERS mapping. Corresponding (a) SEM image, (b) optical image, and (c) SERS intensity map of DioPNPs/*S. aureus*/AgMNPs sandwich architecture. (d) Average SERS spectrum obtained from the different regions of c.

architecture. A corresponding SERS intensity map was created and is shown in Figure 8c. The average SERS spectra obtained from the different regions of Figure 8c are shown in Figure 8d. The results can be attributed to the DTNB Raman reporter molecules brought by the DioPNPs. In the present work, we demonstrated the successful capture, labeling, and subsequent SERS detection of *S. aureus*. As demonstrated in Figure 8, the detection of a single *S. aureus* cell was easily achieved through SERS imaging.

3. CONCLUSIONS

This study is the first to demonstrate a fast, highly sensitive, specific, and low-cost magnetically assisted SERS bioassay for the single-cell detection of *S. aureus* based on aptamer recognition. AgMNPs and a novel SERS tag, DioPNPs, were well-designed and successfully synthesized in accordance with the requirements of *S. aureus* detection. Under the optimized aptamer density and linker length, capture-aptamer-modified AgMNPs can achieve favorable bacteria arrest (up to 75%). The LOD of the proposed biosensor for *S. aureus* is 10 cells/mL by using the conventional Raman spectroscopy. Besides, a good linear relationship is observed from 10^1 to 10^5 cells/mL *S. aureus* concentration, and the correlation coefficient is calculated to be 0.9558. With the help of the newly developed SERS mapping technique, the single-cell detection of *S. aureus* is easily achieved. This SERS bioassay can be extended to the detection of a wide variety of bacterial pathogens or even cells by using the corresponding aptamers. In the future, we expect our proposed bioassay to have important implications for pathogenic bacteria detection in clinical diagnosis and biomedical research.

4. EXPERIMENTAL METHODS

4.1. Chemicals and Materials. Polyethylenimine (PEI, 25 K), trisodium citrate (TSC), 11-mercapto-1-undecanol (MU), 11-mercaptoundecanoic acid (MUA), N-hydroxysuccinimide (NHS), N-(3-dimethylaminopropyl)-N′-ethylcarbodiimide hydrochloride (EDC), ascorbic acid (AA), hexadecyltrimethylammonium bromide (CTAB), 5,5-dithiobis-(2-nitrobenzoic acid) (DTNB), polyvinylpyrrolidone (PVP, 40 K), and Tween 20 were purchased from Sigma-Aldrich. Methanol, ethanol, tungstophosphoric acid, $FeCl_3{\cdot}6H_2O$, $MnCl_2{\cdot}4H_2O$, ethylene glycol (EG), diethylene glycol (DEG), sodium acetate anhydrous (NaOAc), dimethyl silicone oil, $HAuCl_4{\cdot}4H_2O$, sodium borohydride ($NaBH_4$), silver nitrate, formaldehyde (36−38%, wt %), ammonia solution (25−28%, wt %), ethanolamine, hydrochloric acid (36−40%, wt %), NaOH, and $MgCl_2{\cdot}6H_2O$ were purchased from Sinopharm Chemical Reagent Co., Ltd. (Shanghai). PBS buffer (1× , pH 7.4, calcium-free, magnesium-free) was obtained from Life Technologies. All chemicals were of analytical grade and were utilized as received unless mentioned otherwise. All aqueous solutions were prepared with Millipore ultrapure water (purified with Milli-Q system, 18.2 MΩ cm^{-1}). The clinical isolation strain of *S. aureus* (04018) and the commercial *E. coli* (BL21) were provided by Shao's group.[41] The aptamers that can specifically recognize *S. aureus* were synthesized by Sangon Biotech (Shanghai) and are shown in Table S1.[41] FITC-labeled aptamers were used for fluorescence microscopy. Polished silicon substrates (3 in.) were purchased from China Electronics Technology Group Corporation, no. 46 Research Institute (Tianjin).

4.2. Bacteria Sample Preparation and Harvest Conditions. The clinical isolation strain of *S. aureus* (04018) and commercial *E. coli* (BL21) were provided by Shao's group.[41] These two kinds of bacteria were cultured overnight at 37 °C in trypicase soy broth and LB medium, respectively. Subsequently, 100 μL of the bacterial culture was removed, diluted 100 000 times with medium, coated on the agar

DOI: 10.1021/acsami.5b06446
ACS Appl. Mater. Interfaces 2015, 7, 20919−20929

plates, and cultured at 37 °C for 24 h. The number of colony forming units was counted. The remaining bacteria were then harvested through centrifugation at 8000 g for 10 min at 4 °C, and the sediment of bacteria was washed with PBS three times. The cells were then fixed with 90% (v/v) methanol at −20 °C for 10 min and then with absolute methanol at −20 °C overnight. All the bacteria were preserved in absolute methanol at −20 °C and then washed with PBS before use. The concentration of the bacteria was also determined by measuring the optical density (OD) at 600 nm (OD_{600} = 1.0 is approximately 1.5 × 10^8 cells/mL).

4.3. Confocal Imaging of *S. aureus* Bound with FITC-Labeled Aptamers. The FITC-labeled aptamers (250 nM, PBSM) were incubated under protection from light with 100 μL of the bacterial suspension with an OD_{600} of 1.0 under shaking conditions (800 rpm, 37 °C) for 45 min. The bacteria were separated by three rounds of centrifugation at 4500 rpm for 5 min remove any excess free aptamers. The bacterial sediment was redispersed in 100 μL of ethanol. A 20 μL aliquot of above-mentioned bacteria−aptamers suspension in ethanol was dropped on a glass slide and then dried in a light-resistant container. Imaging of the bacteria was carried out with a confocal laser-scanning microscope (FV 1000, Olympus) under a 488 nm excitation laser and visible light.

4.4. Synthesis of Monodispersed Ag-Coated Magnetic NPs and Their Conjugation with Aptamer 1. Superparamagnetic ferrite NPs ($MnFe_2O_4$, ∼170 nm) were synthesized by a solvothermal reaction following the method developed by Leung with some modifications.[37] In brief, $FeCl_3{\cdot}6H_2O$ (4/3 mmol, 360 mg) and $MnCl_2{\cdot}4H_2O$ (2/3 mmol, 131.94 mg) were dissolved in a mixture of EG and DEG (V_{EG}/V_{DEG} = 7:13, total volume is 20 mL) in an explosion-proof bottle under magnetic stirring. Then, 2 g of PVP was added to the above solution, and the solution was heated at 120 °C for approximately 10 min to give a transparent solution. Finally, heating was stopped, and 1.5 g of NaOAc was added into the above solution. After vigorous stirring for an additional 30 min, the obtained homogeneous solution was sealed in a Teflon-lined stainless-steel autoclave (50 mL volume) and then transferred to a vacuum oven, which was preheated to 200 °C. After a 10 h reaction period, the solution was cooled to room temperature, and the obtained ferrite NPs were collected by an external magnet, washed five times with deionized water, and then dried under vacuum at 60 °C for 4 h.

The Ag shell was coated outside the magnetic NPs ($MnFe_2O_4$) by using the seed-mediated growth method. In this method, 4 nm AuNPs were utilized for attachment onto the amino-group-functionalized magnetic nanoparticles, with Ag^+ reduced onto the surface of the composite NPs for complete Ag shell encapsulation. The surface amination of the magnetic NPs ($MnFe_2O_4$) was achieved via PEI self-assembly under sonication. Typically, 0.25 g of PEI was dissolved in deionized water (50 mL) by ultrasonication for 10 min. Subsequently, 0.1 g of the prepared $MnFe_2O_4$ NPs were added into the above-mentioned PEI solution under sonication for another 20 min, during which PEI gradually self-assembled on the $MnFe_2O_4$ NPs. The resulting $MnFe_2O_4$@PEI NPs were magnetically separated and rinsed five times with deionized water. Meanwhile, 4 nm Au seed was synthesized following the method described by Murphy with some modification.[42] In brief, 20 mL of $HAuCl_4$ (5 mM) and 20 mL of TSC (5 mM) were added to 360 mL of deionized water and then vigorously stirred. Afterward, 10 mL of freshly prepared $NaBH_4$ (0.1 M) was added, and the solution color changed from colorless to orange. The solution was stirred for 4 h at room temperature, and the resulting spherical AuNPs were approximately 4 nm in diameter. The prepared PEI-modified $MnFe_2O_4$ NPs and 4 nm AuNPs were mixed and then sonicated for 1 h to form $MnFe_2O_4$@PEI−AuNPs via electrostatic interaction before they were magnetically separated from the solution and rinsed three times with deionized water. Finally, a continuous Ag shell grew outside the magnetic NPs with the Au seeds electrostatically absorbed on the surface of $MnFe_2O_4$ as nuclei. In brief, 2 mg of $AgNO_3$ and 300 mg of PVP were dispersed in 200 mL of deionized water; then, 10 mg of Au seed-decorated $MnFe_2O_4$ NPs were added to the solution. Subsequently, 150 μL of formaldehyde and 300 μL of ammonia solution were added under vigorous sonication at 30 °C. The $MnFe_2O_4$@Ag core−shell NPs were obtained within 5 min. The products were magnetically separated and rinsed five times with deionized water to remove the excess PVP.

AgMNPs ($MnFe_2O_4$@Ag) were carboxyl-group-functionalized and then conjugated with amino aptamer via the universal method. In this method, EDC/NHS was employed to form an active ester that can rapidly couple with amines on target aptamers. In brief, AgMNPs (5 mg/mL) were incubated overnight with vigorous sonication in an ethanol solution containing 1 mM MUA and 1 mM MU before washing with ethanol five times to remove free MUA and MU. Finally, EDC (100 μL, 10 mM) and NHS (20 μL, 0.1 M) were added to 100 μL of the solution containing carboxylated AgMNPs (5 mg/mL), followed by the addition of PBST solution until the total volume reached 1 mL. The mixture was shaken for 15 min (850 rpm, 25 °C). A 25 μL aliquot of aptamer 1 solution (10 μM in PBS) was added, and the mixture was shaken for 2 h. The products were magnetically separated and rinsed three times with deionized water to remove the excess aptamers. To avoid nonspecific absorption, the aptamer-1-conjugated AgMNPs were blocked with ethanolamine (1%, v/v) for 1 h under shaking conditions (850 rpm, 25 °C). After being magnetically separated and washed with deionized water three times, the final precipitate was dispersed in 100 μL of PBS solution for further use.

4.5. Synthesis of AuNR−DTNB@Ag−DTNB Core−Shell Plasmonic NPs and Their Conjugation with Aptamer 2. AuNRs were synthesized following the surfactant-assisted, seed-mediated method developed by Nikoobakht with some modifications.[39] In brief, the seed solution was prepared by adding 2.5 mL of $HAuCl_4$ (0.5 mM) into 2.5 mL of CTAB solution (0.2 M), and 300 μL of freshly prepared $NaBH_4$ (0.01 M) was then added under magnetic stirring (500 rpm, 29 °C) for 1 min. As a result, a brownish-yellow solution was formed. After the stirring was stopped, the resulting seed solution was kept at 29 °C for 1 h before use. To synthesize AuNRs with an aspect ratio of approximately 4, 20 mL of $HAuCl_4$ (1 mM) was added into 20 mL of CTAB solution (0.2 M); after gentle mixing of the solution, 0.4 mL of silver nitrate solution (0.01 M) was added and mixed. Then, 0.38 mL of HCl (2 M) was added and mixed. Subsequently, 0.32 mL of AA (0.1 M) was mixed with the solution before the seed solution (140 μL) was added. Finally, the mixture was placed into a water bath and kept undisturbed at 29 °C for 12 h without any further stirring until the color change was complete. AuNRs were purified three times through centrifugation at 7500 rpm for 6 min to remove any excess reagents and then further purified once through centrifugation at 2500 rpm for 3 min to remove large NPs.

DTNB-functionalized AuNRs (AuNR−DTNB) were prepared according to the following procedure. First, 10 μL of freshly prepared DTNB ethanol solution (10 mM) was added into 10 mL of the as-prepared AuNRs solution, and the resultant mixture was vigorously stirred at 30 °C for 1 h with an ultrasonic machine (45 kHz). The resulting solution was centrifuged at 7500 rpm for 6 min to remove the excess DTNB molecules, and the precipitate was redispersed in 10 mL of deionized water.

Encapsulation with an outer Ag shell of the DTNB-functionalized AuNRs was achieved following a previously reported method with some modifications.[40] In brief, CTAB (72.8 mg) was dissolved in 6 mL of purified AuNR−DTNB solution through sonication, and the solution was then transferred to a magnetic stirrer (700 rpm, 29 °C). Subsequently, 54 μL of freshly prepared AA (0.1 M) was added, followed by the addition of silver nitrate solution (27 μL, 0.01 M). Finally, 240 μL of NaOH solution (0.1 M) was added to elevate the pH to above 10, thus initiating the Ag ion reduction reaction. After 2 min, the color change was complete, and the solution was centrifuged twice at 7500 rpm for 6 min to remove the excess reagents. The final precipitate was redispersed in 6 mL of deionized water.

The preparation of DTNB-functionalized AuNR−DTNB−Ag is almost identical to that of the DTNB-functionalized AuNRs described above.

The *S. aureus* binding aptamer, aptamer 2 (10 μM in PBS), was used to coat the novel SERS tag (DioPNPs) through standard EDC coupling between the DTNB−COOH group and amino group of the aptamer. In brief, 500 μL of DioPNPs was mixed with 20 μL of freshly

DOI: 10.1021/acsami.5b06446
ACS Appl. Mater. Interfaces 2015, 7, 20919−20929

prepared EDC solution (7 mg/mL), and the mixture was shaken for 15 min (850 rpm, 25 °C). Subsequently, 25 μL of the aptamer 2 solution (10 μM in PBS) and 500 μL of the PB buffer (10 mM, pH 7.4) were added, and the mixture was then shaken for 1 h (850 rpm, 25 °C). The nonspecific absorption sites on the surfaces of aptamer-2-conjugated DioPNPs were blocked with ethanolamine (1%, v/v) for 1 h under the same shaking condition. After being separated by centrifugation (7500 rpm, 6 min) and washed twice with PBST, the final precipitate was dispersed in 500 μL of PBS for further use.

4.6. SERS Detection Experiment Details. In a typical experiment, 15 μL of AgMNPs conjugated with aptamer 1 was added to a 1.5 mL centrifuge tube. The AgMNPs were washed once with 0.05% (v/v) T-20 and then magnetically collected. Subsequently, 1 mL of the bacterial suspension (10^6 cells/mL in PBST) and 50 μL of PBSM buffer (1× PBS, 100 mM $MgCl_2$, pH 7.4) were sequentially added. The mixture was incubated with shaking for 45 min (850 rpm, 37 °C). The resulting bacteria−AgMNPs complexes were magnetically separated and rinsed three times with PBST to remove the excess free bacteria. After the washing procedure, 100 μL of aptamer-2-conjugated DioPNPs, 10 μL of PBSM buffer (1× PBS, 100 mM $MgCl_2$, pH 7.4), and 100 μL of PBST buffer (1× PBS, 0.05% T−20) were sequentially added before the mixture was incubated for another 45 min at the same shaking condition. The resulting DioPNPs/bacteria/AgMNPs complexes were washed three times with PBST buffer and then resuspended in 50 μL of ethanol. Finally, 2.5 μL of the above DioPNPs/bacteria/AgMNPs suspension in ethanol was dropped on a silicon substrate. After drying in air, SERS spectroscopy and imaging of the sample were conducted.

4.7. Raman Spectroscopy and Imaging. Raman spectra were collected using a Thermo Fisher DXRxi Raman imaging microscope equipped with a laser operating at a wavelength of 780 nm. Incident radiation was coupled into an Olympus BX51 optical microscope and focused to a 0.7 μm diameter spot through a 100× objective. Raman spectra were recorded with 2 mW laser power, 50 μm aperture slit, and 0.05 s exposure time. Each measured Raman spectrum was an average of 32 experimental microscans. In the Raman mapping experiments, a fine set of grid points within an area of interest was defined, and the image pixel size was set to 0.1 μm. A full Raman spectrum was acquired at each grid point. Upon completion of the mapping, Raman intensity maps were prepared by fitting the corresponding spectra with the reference spectrum and removing the associated background.

4.8. Instrumentation. TEM images were obtained using a Hitachi H-7650 microscope operating at 80 kV. High-resolution TEM (HRTEM) images and EDS spectra were acquired on a JEOL 2010 microscope operating at 200 kV. Field-emission scanning electron microscopy (FE-SEM) images were taken on a FEI NOVA NanoSEM430 microscope operating at 10 kV. UV−vis spectra were obtained using a Shimadzu UV−2600 spectrometer. Confocal fluorescence imaging was carried out with a confocal laser-scanning microscope (FV 1000, Olympus). The green fluorescence signal of FITC was detected using excitation/emission wavelengths at 488/520 nm. Powder XRD patterns of the products were investigated on a Japan Rigaku D/max 2550 VB/PC rotation anode X-ray diffractometer. Magnetic characterization was conducted with a superconducting quantum interference devices (SQUID) magnetometer (MPMS-XL-7, Quantum Design, USA) at 300 K.

4.9. Finite-Difference Time-Domain Simulation. Numerical simulations were carried out with the FDTD method provided by FDTD Solutions (Lumerical) to obtain the extinction spectra of AuNR and AuNR@Ag. The dielectric functions of Au and Ag were properly fitted using Lumerical's multi-coefficient model in the wavelength range of simulation. In all calculations, AuNR or AuNR@Ag was modeled on the basis of the TEM images, and the nanostructure was enclosed in the simulation region with perfectly matched layer boundary conditions in all three dimensions. A 3D nonuniform mesh was used, and the maximum mesh step was set to 0.5 nm. A total-field scattered-field source was used to simulate the interaction between the propagating plane wave source and the nanorod. The refractive index of the surrounding medium (water) was set to 1.33. The extinction cross section for longitudinal polarization was calculated.

■ ASSOCIATED CONTENT

Supporting Information

The Supporting Information is available free of charge on the ACS Publications website at DOI: 10.1021/acsami.5b06446.

Secondary structure of aptamers; electron microscopy images of *S. aureus* (04018) cultured overnight; EDS spectrum of $MnFe_2O_4$@PEI-AuNPs; Ag shell formation process on magnetic nanoparticles; UV−visible spectra of the synthesized magnetic nanoparticles; agarose-gel electrophoresis bands of in situ AgMNPs−aptamer 1 PCR amplification; LSPR wavelength adjustment of PNPs; FDTD-simulated LSPR spectra of AuNR and AuNR−Ag; EDS spectrum of AuNR-DTNB@Ag; Electron microscopy images of DioPNPs/*S. aureus*/AgMNPs sandwich architecture; and aptamer sequences used in this study. (PDF)

■ AUTHOR INFORMATION

Corresponding Authors

*Tel.: +86-731-84574958. E-mail: ptdong@nudt.edu.cn.
*Tel.: +86-10-66931422-5. E-mail: ruixiao203@sina.com.
*Tel.: +86-10-66932211. E-mail:sqwang@bmi.ac.cn.

Author Contributions

J.W., X.W., and C.W. contributed equally to the creation of this work.

Notes

The authors declare no competing financial interest.

■ ACKNOWLEDGMENTS

This work was funded by National Natural Science Foundation of China under grant no. 51475468 and the Foundation of State Key Laboratories of Transducer Technology under grant no. SKT1201. We thank Dr. Le Su, Thermo Fisher Scientific, Inc., for helping to conduct SERS mapping.

■ REFERENCES

(1) Miller, L. S.; Cho, J. S. Immunity against Staphylococcus Aureus Cutaneous Infections. *Nat. Rev. Immunol.* **2011**, *11*, 505−518.

(2) Chang, Y. C.; Yang, C. Y.; Sun, R. L.; Cheng, Y. F.; Kao, W. C.; Yang, P. C. Rapid Single Cell Detection of Staphylococcus Aureus by Aptamer-Conjugated Gold Nanoparticles. *Sci. Rep.* **2013**, *3*, 1863.

(3) Chang, T. C.; Huang, S. H. An Enzyme-Linked Immunosorbent Assay for the Rapid Detection of Staphylococcus Aureus in Processed Foods. *J. Food Prot.* **1994**, *57*, 184−189.

(4) Cheng, J.-C.; Huang, C.-L.; Lin, C.-C.; Chen, C.-C.; Chang, Y.-C.; Chang, S.-S.; Tseng, C.-P. Rapid Detection and Identification of Clinically Important Bacteria by High-Resolution Melting Analysis after Broad-Range Ribosomal RNA Real-Time PCR. *Clin. Chem.* **2006**, *52*, 1997−2004.

(5) Moore, D. F.; Curry, J. I. Detection and Identification of Mycobacterium Tuberculosis Directly from Sputum Sediments by Ligase Chain Reaction. *J. Clin. Microbiol.* **1998**, *36*, 1028−1031.

(6) Abbaspour, A.; Norouz-Sarvestani, F.; Noori, A.; Soltani, N. Aptamer-Conjugated Silver Nanoparticles for Electrochemical Dual-Aptamer-Based Sandwich Detection of Staphylococcus Aureus. *Biosens. Bioelectron.* **2015**, *68*, 149−155.

(7) Duan, N.; Wu, S.; Zhu, C.; Ma, X.; Wang, Z.; Yu, Y.; Jiang, Y. Dual-Color Upconversion Fluorescence and Aptamer-Functionalized Magnetic Nanoparticles-Based Bioassay for the Simultaneous Detection of Salmonella Typhimurium and Staphylococcus Aureus. *Anal. Chim. Acta* **2012**, *723*, 1−6.

DOI: 10.1021/acsami.5b06446
ACS Appl. Mater. Interfaces 2015, 7, 20919−20929

(8) Yuan, J.; Wu, S.; Duan, N.; Ma, X.; Xia, Y.; Chen, J.; Ding, Z.; Wang, Z. A Sensitive Gold Nanoparticle-Based Colorimetric Aptasensor for Staphylococcus Aureus. *Talanta* **2014**, *127*, 163−168.
(9) Sung, Y. J.; Suk, H. J.; Sung, H. Y.; Li, T.; Poo, H.; Kim, M. G. Novel Antibody/Gold Nanoparticle/Magnetic Nanoparticle Nanocomposites for Immunomagnetic Separation and Rapid Colorimetric Detection of Staphylococcus Aureus in Milk. *Biosens. Bioelectron.* **2013**, *43*, 432−439.
(10) Lin, C. C.; Yang, Y. M.; Liao, P. H.; Chen, D. W.; Lin, H. P.; Chang, H. C. A Filter-Like AuNPs@MS SERS Substrate for Staphylococcus Aureus Detection. *Biosens. Bioelectron.* **2014**, *53*, 519−527.
(11) Drake, P.; Jiang, P.-S.; Chang, H.-W.; Su, S.-C.; Tanha, J.; Tay, L.-L.; Chen, P.; Lin, Y.-J. Raman Based Detection of Staphylococcus Aureus Utilizing Single Domain Antibody Coated Nanoparticle Labels and Magnetic Trapping. *Anal. Methods* **2013**, *5*, 4152.
(12) Singh, A. K.; Senapati, D.; Wang, S.; Griffin, J.; Neely, A.; Candice, P.; Naylor, K. M.; Varisli, B.; Kalluri, J. R.; Ray, P. C. Gold Nanorod Based Selective Identification of Escherichia Coli Bacteria Using Two-Photon Rayleigh Scattering Spectroscopy. *ACS Nano* **2009**, *3*, 1906−1912.
(13) Guven, B.; Basaran-Akgul, N.; Temur, E.; Tamer, U.; Boyaci, I. H. SERS-Based Sandwich Immunoassay Using Antibody Coated Magnetic Nanoparticles for Escherichia Coli Enumeration. *Analyst* **2011**, *136*, 740−748.
(14) Yuan, J.; Yu, Y.; Li, C.; Ma, X.; Xia, Y.; Chen, J.; Wang, Z. Visual Detection and Microplate Assay for Staphylococcus Aureus Based on Aptamer Recognition Coupled to Tyramine Signal Amplification. *Microchim. Acta* **2014**, *181*, 321−327.
(15) Li, J.; Xu, M.; Huang, H.; Zhou, J.; Abdel-Halimb, E.; Zhang, J.-R.; Zhu, J.-J. Aptamer-Quantum Dots Conjugates-Based Ultrasensitive Competitive Electrochemical Cytosensor for the Detection of Tumor Cell. *Talanta* **2011**, *85*, 2113−2120.
(16) Hu, Y. S.; Jeon, J.; Seok, T. J.; Lee, S.; Hafner, J. H.; Drezek, R. A.; Choo, H. Enhanced Raman Scattering from Nanoparticle-Decorated Nanocone Substrates: A Practical Approach to Harness in-Plane Excitation. *ACS Nano* **2010**, *4*, 5721−5730.
(17) Tsoutsi, D.; Montenegro, J. M.; Dommershausen, F.; Koert, U.; Liz-Marzán, L. M.; Parak, W. J.; Alvarez-Puebla, R. A. Quantitative Surface-Enhanced Raman Scattering Ultradetection of Atomic Inorganic Ions: The Case of Chloride. *ACS Nano* **2011**, *5*, 7539−7546.
(18) Porter, M. D.; Lipert, R. J.; Siperko, L. M.; Wang, G.; Narayanan, R. SERS as a Bioassay Platform: Fundamentals, Design, and Applications. *Chem. Soc. Rev.* **2008**, *37*, 1001−1011.
(19) Wang, Y.; Yan, B.; Chen, L. SERS Tags: Novel Optical Nanoprobes for Bioanalysis. *Chem. Rev.* **2013**, *113*, 1391−1428.
(20) Schlucker, S. Surface-Enhanced Raman Spectroscopy: Concepts and Chemical Applications. *Angew. Chem., Int. Ed.* **2014**, *53*, 4756−4795.
(21) Dougan, J. A.; Faulds, K. Surface Enhanced Raman Scattering for Multiplexed Detection. *Analyst* **2012**, *137*, 545−554.
(22) Wang, J. F.; Wu, X. Z.; Xiao, R.; Dong, P. T.; Wang, C. G. Performance-Enhancing Methods for Au Film over Nanosphere Surface-Enhanced Raman Scattering Substrate and Melamine Detection Application. *PLoS One* **2014**, *9*, e97976.
(23) Wu, L.; Wang, Z.; Fan, K.; Zong, S.; Cui, Y. A SERS-Assisted 3D Barcode Chip for High-Throughput Biosensing. *Small* **2015**, *11*, 2798−2806.
(24) Li, D.; Zhang, Y.; Li, R.; Guo, J.; Wang, C.; Tang, C. Selective Capture and Quick Detection of Targeting Cells with SERS-Coding Microsphere Suspension Chip. *Small* **2015**, *11*, 2200−2208.
(25) Li, J. F.; Huang, Y. F.; Ding, Y.; Yang, Z. L.; Li, S. B.; Zhou, X. S.; Fan, F. R.; Zhang, W.; Zhou, Z. Y.; Wu, D. Y.; Ren, B.; Wang, Z. L.; Tian, Z. Q. Shell-Isolated Nanoparticle-Enhanced Raman Spectroscopy. *Nature* **2010**, *464*, 392−395.
(26) Nie, S.; Emory, S. R. Probing Single Molecules and Single Nanoparticles by Surface-Enhanced Raman Scattering. *Science* **1997**, *275*, 1102−1106.
(27) Cao, Y. C.; Jin, R.; Mirkin, C. A. Nanoparticles with Raman Spectroscopic Fingerprints for DNA and RNA Detection. *Science* **2002**, *297*, 1536−1540.
(28) Tripp, R. A.; Dluhy, R. A.; Zhao, Y. Novel Nanostructures for SERS Biosensing. *Nano Today* **2008**, *3*, 31−37.
(29) Donnelly, T.; Smith, W. E.; Faulds, K.; Graham, D. Silver and Magnetic Nanoparticles for Sensitive DNA Detection by SERS. *Chem. Commun.* **2014**, *50*, 12907−12910.
(30) Mahmoudi, M.; Serpooshan, V. Silver-Coated Engineered Magnetic Nanoparticles Are Promising for the Success in the Fight against Antibacterial Resistance Threat. *ACS Nano* **2012**, *6*, 2656−2664.
(31) Hu, H.; Wang, Z.; Pan, L.; Zhao, S.; Zhu, S. Ag-Coated Fe3O4@SiO2 Three-Ply Composite Microspheres: Synthesis, Characterization, and Application in Detecting Melamine with Their Surface-Enhanced Raman Scattering. *J. Phys. Chem. C* **2010**, *114*, 7738−7742.
(32) Han, B.; Choi, N.; Kim, K. H.; Lim, D. W.; Choo, J. Application of Silver-Coated Magnetic Microspheres to a SERS-Based Optofluidic Sensor. *J. Phys. Chem. C* **2011**, *115*, 6290−6296.
(33) Zhao, B.; Shen, J.; Chen, S.; Wang, D.; Li, F.; Mathur, S.; Song, S.; Fan, C. Gold Nanostructures Encoded by Non-Fluorescent Small Molecules in Polya-Mediated Nanogaps as Universal SERS Nanotags for Recognizing Various Bioactive Molecules. *Chem. Sci.* **2014**, *5*, 4460−4466.
(34) Jun, B. H.; Noh, M. S.; Kim, J.; Kim, G.; Kang, H.; Kim, M. S.; Seo, Y. T.; Baek, J.; Kim, J. H.; Park, J.; Kim, S.; Kim, Y. K.; Hyeon, T.; Cho, M. H.; Jeong, D. H.; Lee, Y. S. Multifunctional Silver-Embedded Magnetic Nanoparticles as SERS Nanoprobes and Their Applications. *Small* **2010**, *6*, 119−125.
(35) Lien, K.-Y.; Hung, L.-Y.; Huang, T.-B.; Tsai, Y.-C.; Lei, H.-Y.; Lee, G.-B. Rapid Detection of Influenza a Virus Infection Utilizing an Immunomagnetic Bead-Based Microfluidic System. *Biosens. Bioelectron.* **2011**, *26*, 3900−3907.
(36) Wen, C.-Y.; Wu, L.-L.; Zhang, Z.-L.; Liu, Y.-L.; Wei, S.-Z.; Hu, J.; Tang, M.; Sun, E.-Z.; Gong, Y.-P.; Yu, J.; Pang, D.-W. Quick-Response Magnetic Nanospheres for Rapid, Efficient Capture and Sensitive Detection of Circulating Tumor Cells. *ACS Nano* **2014**, *8*, 941−949.
(37) Xuan, S.; Wang, F.; Wang, Y.-X. J.; Yu, J. C.; Leung, K. C.-F. Facile Synthesis of Size-Controllable Monodispersed Ferrite Nanospheres. *J. Mater. Chem.* **2010**, *20*, 5086.
(38) Wang, Z.; Zong, S.; Li, W.; Wang, C.; Xu, S.; Chen, H.; Cui, Y. SERS-Fluorescence Joint Spectral Encoding Using Organic-Metal-QD Hybrid Nanoparticles with a Huge Encoding Capacity for High-Throughput Biodetection: Putting Theory into Practice. *J. Am. Chem. Soc.* **2012**, *134*, 2993−3000.
(39) Nikoobakht, B.; El-Sayed, M. A. Preparation and Growth Mechanism of Gold Nanorods (NRs) Using Seed-Mediated Growth Method. *Chem. Mater.* **2003**, *15*, 1957−1962.
(40) Xiang, Y.; Wu, X.; Liu, D.; Li, Z.; Chu, W.; Feng, L.; Zhang, K.; Zhou, W.; Xie, S. Gold Nanorod-Seeded Growth of Silver Nanostructures: From Homogeneous Coating to Anisotropic Coating. *Langmuir* **2008**, *24*, 3465−3470.
(41) Cao, X.; Li, S.; Chen, L.; Ding, H.; Xu, H.; Huang, Y.; Li, J.; Liu, N.; Cao, W.; Zhu, Y.; Shen, B.; Shao, N. Combining Use of a Panel of ssDNA Aptamers in the Detection of Staphylococcus Aureus. *Nucleic Acids Res.* **2009**, *37*, 4621−4628.
(42) Busbee, B. D.; Obare, S. O.; Murphy, C. J. An Improved Synthesis of High-Aspect-Ratio Gold Nanorods. *Adv. Mater.* **2003**, *15*, 414−416.

DOI: 10.1021/acsami.5b06446
ACS Appl. Mater. Interfaces 2015, 7, 20919−20929